

An Experimental Study of Downfacing Surfaces in Selective Laser Melting

Joe Joseph Babu, Mehrshad Mehrpouya, Thomas C. Pijper, Gydo Willemsen, and Tom Vaneker*

This article presents an investigative study to evaluate the effect of process parameters on surface roughness and dimensional accuracy of downfacing surfaces. The material used in the study is Corrax steel and is fabricated using selective laser melting (SLM) technology. The fabrication process of the downfacing surface is different from the fabrication of the main or core region due to the poor thermal conductivity of loose powder particles beneath each layer. The processing parameters, namely, laser scanning speed, laser power, and layer reference, are investigated using a full factorial design of experiments method to discover their influence on surface roughness and dimensional deviation. Results show that the investigated factors are significantly affecting the quality of downfacing surfaces and controlling them will greatly influence achieving required surface properties.

geometric complexity and production volume is low.^[5,6] Selective laser melting (SLM) technology, also known as direct metal laser melting (DMLM), is a type of powder bed fusion (PBF) process and typically consists of a laser system, scan head, gas flow system, build platform, a baseplate, a powder spreading system, a feed container, and an overflow container. SLM uses high intensity, high-power infrared laser as an energy source to melt the powder layer-by-layer in accordance with the computer-aided design (CAD) data. SLM is a proven technology capable of producing near-net-shape parts with a density greater than 99.9%. **Figure 1** exemplifies the principle components in an SLM system.

There are various operational parameters in the SLM system with a direct impact on the surface quality of 3D printed products, including energy density, scan speed, laser spot size, layer thickness, hatch spacing, scanning strategy, and so on.^[7–10] From these, it is important to identify and optimize the processing parameters that allow for minimizing the surface roughness and preventing premature failure from surface-initiated cracking.^[11] Surface roughness also increases friction between moving parts, and can increase the built-up of surface contaminants (very unwanted for applications such as food or medical). Surface roughness has a direct correlation with the fatigue life of a product^[12,13] so that decreasing surface roughness enhances the fatigue limit of a printed part.^[14] Consequently, it is essential to understand, predict, and control the surface roughness for AM process.

Various studies have investigated the surface roughness of top surfaces and vertical surfaces. However, there are a few studies on the quality of inclined surfaces of SLM-fabricated parts including upskin and downskin surfaces. This is the case, particularly for downskin surfaces, the formation of which is the more complicated process. Strano et al.^[15] have developed mathematical models for both the staircase effect and the impact of attached particles with the limitation of not taking material properties and characteristics into account. Hence, it is inadequate for exposing the mechanisms of thermal behavior, the interaction between the materials and the laser, and their influence on surface conditions. Mumtaz et al.^[11] investigated the impact of process parameters on surface quality on sloping planes of Inconel 625 wall parts. Results revealed that a low repetition rate, high peak power, and high scanning speed help in decreasing incline surface roughness.


1. Introduction

Additive manufacturing (AM) technology, well-known as 3D printing, is a unique technology for the fabrication of customized parts directly from the computer-aided design (CAD) design. Today, additively manufactured parts can be found throughout the entire product lifecycle, from preproduction (e.g., rapid prototyping) to full-scale production, as well as in tooling applications and postproduction customization.^[1–4] Metal AM offers design freedom with the ability to manufacture parts from a wide range of classic and functional materials (metals, ceramics) and it is mainly used for industrial applications where there is high

J. J. Babu, M. Mehrpouya, T. Vaneker
Faculty of Engineering Technology
University of Twente
P.O. Box 217, 7500 AE Enschede, The Netherlands
E-mail: t.vaneker@utwente.nl

T. C. Pijper, G. Willemsen
Philips Consumer Lifestyle
Oliemolenstraat 5, 9203 ZN Drachten, The Netherlands

T. C. Pijper
Innovation Cluster Drachten
Nipkowlaan 5, 9207 JA Drachten, The Netherlands

 The ORCID identification number(s) for the author(s) of this article can be found under <https://doi.org/10.1002/adem.202101562>.

© 2022 The Authors. Advanced Engineering Materials published by Wiley-VCH GmbH. This is an open access article under the terms of the Creative Commons Attribution License, which permits use, distribution and reproduction in any medium, provided the original work is properly cited.

DOI: 10.1002/adem.202101562

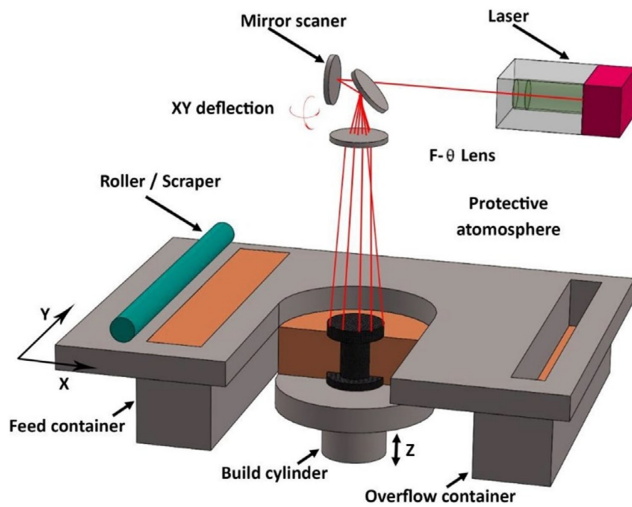


Figure 1. A schematic of an SLM system that locally fuses metal powder on a preheated platform using a laser head, and then the roller adds additional powder layer-by-layer to create the final product. Reproduced with permission.^[38] Copyright 2021, Elsevier.

Downfacing surfaces are supported by loose powder below them instead of solidified material. The thermal conductivity of powder material is roughly 100 times lower than solid material; thus, it hampers the cooling of the melt pool, causing it to become longer, wider, and deeper. Consequently, the liquid metal is subjected to various factors (capillarity forces, gravity, and Marangoni convection flow) which result in an unstable melt pool that sinks into the loose powder bed and leads to dross formation, which, in turn, results in poor surface quality and geometrical accuracy.^[16] The amount of dross depends on the base material and applied process parameters. Dross has an irregular shape and its formation is a very hard-to-control phenomenon due to the random nature of powder particles' packing.^[17] Yadroitsev et al.^[18] mentioned that the major fabricating defects in downfacing structures are dross formation, the staircase effect, and balling.

Balling phenomenon is a challenging issue in the SLM system and it is due to a complex interaction between mass, multimode heat, and momentum transfer.^[19] Balling is a separated part of the melt pool into small pieces. During the SLM process, the molten track created by the laser has a shrinking tendency in order to reduce the surface energy due to the effect of surface tension. Therefore, the influence of high temperature between various volumes of the molten parts and material creates the surface tension in the molten pool. This shrinkage leads to the balling phenomenon and takes place readily during the SLM fabrication process, which is damaging to the quality of the SLM manufactured part. Kruth et al. declared that the balling phenomenon occurs when the melt pool surface enlarges more than a sphere with a similar volume.^[16] Moreover, low velocity in the melt pool and cold powder bed is favorable for balling effect due to poor wetting conditions.^[15] The balling outcome restricts the resolution of the SLM process due to the formation of disconnected tracks, possibly resulting in unmelted material or pores in the component, which may decrease the mechanical

strength of the component.^[11] The difference between the inclined surface profile, as described by the CAD file, and the surface profile causes the staircase effect. The exact geometry on inclined or curved surfaces of each step edge is dependent on process and material, and hence cannot be defined by rectilinear steps.^[15] As an additional effect, the staircase effect increases the attachment of the powder particles to the downfacing parts and creates heterogeneity on the surface of the SLM-fabricated parts.

Calignano^[20] and Cloots et al.^[21] investigated the SLM printing of downfacing surfaces such as ledges, convex radii, and concave radii feature with AlSi10Mg and Ti6Al4V. Calignano concluded that the downward-sloping faces can be built without supports at angles up to 30° at the expense of having a higher surface roughness and overhanging structures should not be considered in the design as much as possible. Nevertheless, it is necessary to design special support structures when they cannot be avoided in order to have the minimum possible contact with the overhang. Cloots et al. divided the part into two zones, namely, core and downfacing zone. The process parameters can be tuned individually for each zone to attain the required properties (typically low residual stresses, high surface quality, and/or high relative density). This helps in achieving a more stable melt track for the downfacing area as shown by Chen et al.,^[22] by simulation, which reduces dross formation and improves the geometry. In addition, this study investigated the number of layers required for a stable overhang to minimize the need for the supports altogether. The quality of the overhang was found to be improved by increasing the scan speed (at low energy density). An overhang of 20° without support was achieved. The volumetric energy density of the key parameter strongly affected the border and the surface of overhang parts.

Modeling and simulation of the SLM process can help explain the experimental observations and optimize the fabrication systems. Experimental study of physics and phenomena is time-consuming and expensive. An impressive 3D mesoscopic model was developed by Khairallah et al.^[23] in 2014, which gave new insights into the surface tension effects on topology and heat transfer. The importance of surface tension effects in melt pool dynamics was discussed in this article. They created a single-track SLM process in 3D using a hybrid finite element and finite volume formulation. It was concluded that surface tension effects are, in fact, the driving forces in the SLM process. This hybrid finite element method-finite volume method (FEM-FVM) approach, however, neglected the effects of wetting, thermal gradients, and so on. Another mesoscale simulation of laser powder bed fusion (LPBF) was carried out by Afrasiabi et al.,^[24] using the smoothed particle hydrodynamics (SPH) method. It was shown to reduce the computational cost of SPH LPBF simulations via spatial adaptivity. More experiments are required to validate the numerical model data.

Xiang et al.^[25] studied the quality of slope surfaces using finite element simulation and experimental verification. They found as the angle of inclination from the horizontal base plate increases, surface quality increases, and dimensional deviation decreases. Shi et al.^[26] found that lower scanning power and the use of an island scanning strategy (used to reduce stresses) were more beneficial for printing overhangs with angles below the critical angle. The effect of heat conduction is very critical when the angle between the top plane of the base plate and the overhanging

surface is less than 45°. The isolating impact of the powder is a dominating factor for angles below 45° that hinders the dissipation of the heat from the building plane to surrounding material.^[22]

SLM process is inherently a multiscale problem as it involves a variety of complex phenomena. The entire properties and characteristics of the laser-directed melting of powder and printing process are practically difficult to simulate owing to the processing time as well as the complexity of phenomena. These complexities include, and are not limited to, laser–powder interactions, material phase transitions, violent free-surface flows, Marangoni effect, radiation, recoil pressure, compressible gas flow, strong evaporation, hot plasma formation, gas bubbles, surface tension and its effect on the topology and heat conduction, nature of the powder bed, and so on. Although the AM process simulation generates excellent insights, the issue with their computational effort is still an open question.

Overall, the downskin surface roughness is normally higher than the upskin surface roughness, which causes a challenging issue for the design of the processing parameter. Wang et al.^[27] found that a lower scanning speed of 200 mm s⁻¹ resulted in a rougher downskin surface due to dross formation and more severe warpage compared to the scanning speed of 600 mm s⁻¹. As a result, a higher speed is recommended to improve this effect.^[22] This can be achieved with in situ monitoring and further correction,^[28] or through gradually changing laser exposure parameters for the part's main volume (core) to those designed exclusively for downskin surfaces.^[29] Dross formation is considered the most unpredictable and hard-to-control defect occurring in SLM and results in high surface roughness and geometrical inaccuracies for overhanging surfaces.^[30] Typically, the roughness is more pronounced on downward-facing surfaces having an angle below 45° for the build platform.

An additional source of surface roughness is support structures, the use of which is inevitable when building steeper angles and the removal whereof contributes to the reduced surface quality. Although it is possible to produce parts with complex shapes using SLM, structural supports are typically needed in order to avoid the failure of unsupported overhanging parts, including various other complex forms of features. Support structures are used for heat conduction to the base plate and act as a heat sink, and/or to stabilize mechanically the fabricated parts by anchoring its solid material below (earlier printed material or the build plate). Depending on their importance, the support structures can be loosely or strongly connected to the part surface. However, attachment does lead to surface defects in the form of scarring of the part. Even though support is designed to be removed easily, a fragment of it remains attached in the central area and these defects must be removed in postprocessing to achieve the desired final quality.

The present study aims to achieve the optimum process parameters for the SLM printing of Corrax that results in the lowest surface roughness and highest dimensional accuracy. The scope of the research is restricted to the downward-facing region of SLM printed parts and the main question hereby is what factors play a major role in these surface quality metrics.

Table 1. Chemical composition of the Corrax.

Elements	C	Si	Cr	Mn	Ni	Mo	Al	Fe
Amount [%]	0.03	0.3	12.0	0.3	9.2	1.4	1.6	75.17

2. Experimental Section

2.1. Material

The applied material for this experiment is Corrax powder (Uddeholm AM Corrax).^[31] Corrax is a stainless steel AM powder with good corrosion resistance and high hardness that makes it an excellent choice for the tooling industry. **Table 1** shows the chemical composition of Corrax powder.

2.2. Equipment

An SLM 280HL 3D printer manufactured by SLM Solutions Group AG (Lübeck, Germany) is utilized in this work. This system has a build platform with a dimension of 280 × 280 × 365 mm and is equipped with a 400 W ytterbium fiber laser. The laser beam has a focal point diameter of approximately 80 µm. The speed of argon flow across the build chamber in this study is maintained at 18 m/s during the experiment so that it keeps the oxygen level below 0.1%. Also, the build platform temperature is set to 100 °C for this study. A rigorous procedure is used before starting experiments to keep a good quality laboratory practice. This process thoroughly involved cleaning the lens, build chamber, bearing seals and rail, and changing the filter.

2.3. CAD Model and Build Preparation

Two sets of samples with a different overhanging angle of 45° and 40° (from the horizontal line) are designed for the experiment, as shown in **Figure 2a**. The first set of samples with 45° inclination are named A1, A2, A3, and so on. The second set of samples with 40° inclination are named B1, B2, B3, and so on. The samples are arranged on the build plate in the increasing order of magnitude of energy density. The distance between samples is arranged such that, if in case any one of the samples fails in between the printing, the rest of the batch could be continued to print by just turning off the failed one. **Figure 2b** illustrates the arrangement of the samples as the 45° samples are denoted by A and 40° by B.

2.4. Design of Experiments

Before the fabrication of parts, a search for an appropriate “parameter window” is necessary. This parameter window differs according to the type of materials and depends on the material's thermophysical properties. The effect of the main process parameters depends on the combinations of their values. Experiment design should be applied to determine the significance of the parameters, the effect of their interactions, to better understand the process and optimize the parameters window.

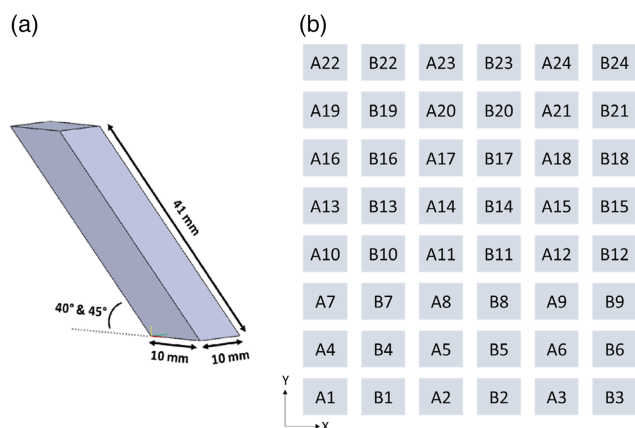


Figure 2. a) CAD model of the designed sample. Two sets of samples are designed. Sample sets A have 45° inclination and sample sets B have 40° inclination from the horizontal plane. b) The arrangement of samples on the build plate. Samples are arranged in the increasing order of designed linear energy density as explained in the section below.

The experiment is designed using “full factorial design.” In statistics, a full factorial experiment is an experiment whose design consists of two or more variables, each of which has distinct possible values or “levels,” and experiments are carried out on all possible combinations of these levels of variables. Factorial designs are more efficient than the one-factor-at-time (OFAT) approach, which varies one parameter at a time. They provide more information at a similar or lower cost. They can find optimal conditions faster than OFAT experiments. In the literature, the laser power, the scanning speed, and interaction between them (energy density) are presented as the most significant input parameters that affect the quality of produced parts. The enhancement of the energy density up to an optimal value changes the viscosity and surface tension of the melted material that finally results in a part with lower surface roughness.^[32]

The experimental study is designed using a “full factorial design” approach based on three main operational parameters including laser power, scan speed, and layer reference (LR). **Table 2** shows a different combination of operational parameters with energy density from 0.0385 to 0.25. As visible, four laser powers, three scan speeds, and two-LR settings are considered in this study.

The downskin region is determined by the LR and angle of inclination in the samples. LR is a parameter that indicates how much area is to be treated as a downskin area and to be scanned with dedicated downskin process parameters. Different sets of parameters are assigned for the fabrication of the core and downskin in the samples. **Figure 3** represents the LR calculation and the width of the downskin could be determined from the sliced image provided by the SLM viewer (a software package by SLM Solutions that visualizes the SLM process from the generated build file). For an LR value of 2, the width of downskins is 0.0709 and 0.0807 mm for samples 45° and 40°, respectively. This increased to 0.1206 and 0.1440 mm for an LR value of 4.

Table 2. The applied operational parameters in this study.

No.	Power [W]	Speed [mm s ⁻¹]	LR	Energy density
1	50	1300	2	0.0385
2	50	1300	4	0.0385
3	50	1050	2	0.0476
4	50	1050	4	0.0476
5	50	800	2	0.0625
6	50	800	4	0.0625
7	100	1300	2	0.0769
8	100	1300	4	0.0769
9	100	1050	2	0.0952
10	100	1050	4	0.0952
11	150	1300	2	0.1154
12	150	1300	4	0.1154
13	100	800	2	0.1250
14	100	800	4	0.1250
15	150	1050	2	0.1429
16	150	1050	4	0.1429
17	200	1300	2	0.1538
18	200	1300	4	0.1538
19	150	800	2	0.1875
20	150	800	4	0.1875
21	200	1050	2	0.1905
22	200	1050	4	0.1905
23	200	800	2	0.2500
24	200	800	4	0.2500

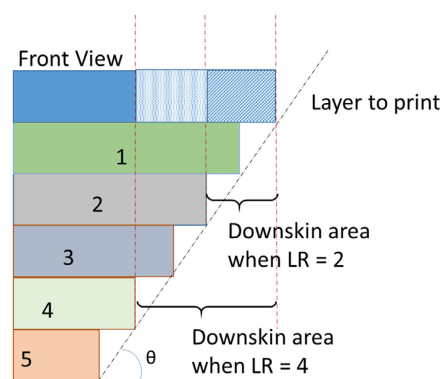


Figure 3. LR calculation (a value of 2 takes two previous layers to calculate the downskin area and correspondingly a value of 4 takes four previous layers).

Various process settings are used for the designed parts so that core is scanned with one set of parameters, while the downskin is scanned with another set of parameters. The core is printed with the default settings which are presented in **Table 3** and provided by SLM GmbH. Therefore, the same core-setting is applied to all the samples, while only the power, scan speed, and LR of the downskin are modified for each sample as shown previously in **Table 2**.

Table 3. Core parameters.

Parameters	Power [W]	Speed [mm s ⁻¹]
Border—volume	100	425
Fill contour—volume	100	420
Hatch—volume	200	720

2.5. Testing Setup

The Mahr LD 120 system is employed for measuring the surface roughness of the printed samples. The roughness measurement is performed according to ISO4288 for each sample at the center of the track and 0.5 mm to the left and right of the track. A force equal to 0.001 N and a traverse speed of 0.5 mm s⁻¹ are applied in this test and the direction of measurement is from the bottom to top of the sample in the build direction.

The dimension of the as-built downskin walls and side walls is measured by Mitutoyo 293-IP54 digital micrometer with a resolution of 1 μm and an accuracy of ±2 μm. Three sets of measurements are taken at five points along the length of the sample at a 7 mm distance apart. The measurement direction is from the bottom to top of the sample in the build direction.

The microscopy evaluation is performed using a ZEISS Stemi 508 stereomicroscope with 8:1 zoom. 3D observation is made through eyepieces. A camera attached to the microscope helps to capture the images in a 2D view. Images captured by the camera are stored on a computer. Software bundled with the microscope is used to measure dimensions.

3. Results and Discussion

3.1. Visual Investigation

All 24 samples are printed based on the aforementioned operational parameters as mentioned in the previous section. **Figure 4** shows the visual appearance of the upskin and downskin surfaces of the fabricated samples and it shows the presence of large

spatter or dross formation. Also, the surface irregularities are observed more in the 40° downfacing surface compared to 45° samples. Accordingly, it indicates a higher surface roughness in the 40° samples than the 45° samples. This is further confirmed by the roughness measurement results. As anticipated, upskin is smoother than downskin, while dross and balling could be seen in all the samples.

3.2. Microscopic Analysis

Figure 5a exemplifies the microstructural view of the downskin surface for the fabricated sample (sample B2). In the melting process, overheating and extra dwell time can cause the formation of keyhole pores.^[33] This figure reveals the formation of ripples and pillar structures in the downskin surface of the samples which was created due to unstable melt dynamics in the printing process. The heights of these pillars are measured as shown clearly in **Figure 5b**. **Figure 5c,d** also demonstrates the presence of melted and unmelted powder particles on the downskin surface in a microstructural view.

Figure 6 reveals the formation of material addition at the tips of some samples. This was observed only for the samples in the second column. Such manufacturing defects may arise due to printed material curling up (often due to slight overheating) at the periphery of the part at some point during the build. Then, during recoating, contact between the recoating mechanism (for the SLM280HL system a composite wiper blade) and curled-up material causes the damage of the former. After this, subsequent recoating actions will show a line (often a shallow depression) in the powder bed on the position of the recoater blade damage. This recoater track is clearly visible in **Figure 6** (the red line on the right side of sample groups 2). This affects build quality and can sometimes even increase the curling-up effect, causing further damage to the recoater blade. The recoater tracks on the powder bed were clearly visible toward the last couple of layers. Fortunately, the recoater damage occurred during the final layers of the print and thus did not affect the print quality of the samples where it mattered.

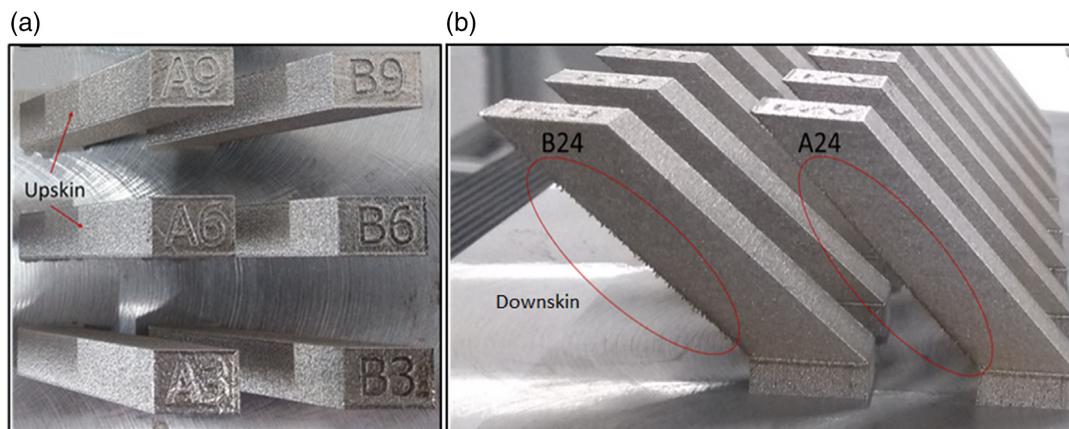


Figure 4. a) Upskin and b) downskin surfaces of the printed samples.

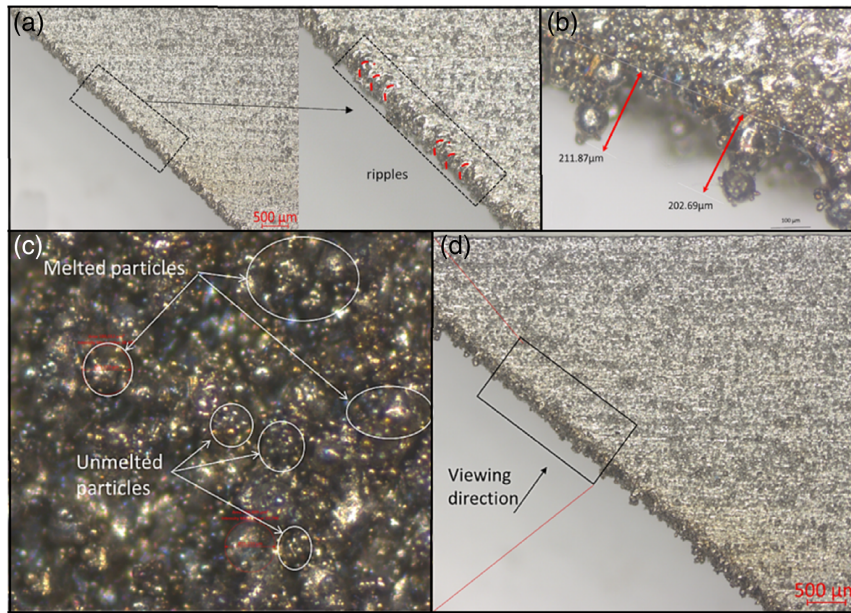


Figure 5. Microstructural characterization of the printed Corrax samples: a) a view on downslope surface ripples creation on the side of the sample, b) creation of pillars and the dimensions, c) melted and unmelted particles in downslope resin, d) and the microstructural view of the particles.

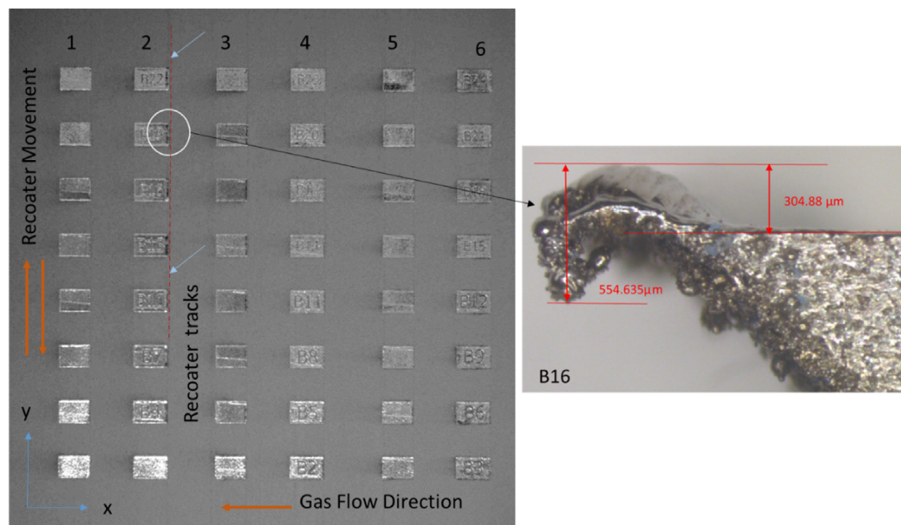


Figure 6. Formation of additional material at the tips of some samples.

3.3. Surface Roughness Evaluation

The melting behavior of the powder in the build chamber is mainly driven by the fluid behavior of the melt pool which is linked to surface tension (Rayleigh instability), viscosity, wetting, thermocapillary effects (Marangoni convection), oxidation, and evaporation. All changes in viscosity within the melt pool might affect largely the shape of the tracks due to variations in viscosity between the solidus and liquidus temperature, and the causing density and smoothness of the parts achieved.

Figure 7 represents the interaction plot of R_a surface roughness for samples A (45°) and B (40°). The interactions are

between power–speed, power–LR, and speed–LR based on the roughness values in Y-axis. It can be seen that the lowest speed of 800 mm s^{-1} and the highest power of 200 W are detrimental to surface quality as they result in the highest surface roughness. For any given power, increasing the scan speed is found to decrease R_a significantly at first till 1050 mm s^{-1} , after which the decrease in R_a becomes less pronounced. This can be seen in both 45° and 40° samples. At 100 W , all scan speeds tested gave the lowest R_a value for both LR values of 2 and 4 (outliers are at 150 W , 800 mm s^{-1} , LR = 4 for A and 150 W , 1300 mm s^{-1} , LR = 2 for B). 1300 mm s^{-1} gave the least surface roughness for LR 2, while 1050 mm s^{-1} gave for LR 4. The

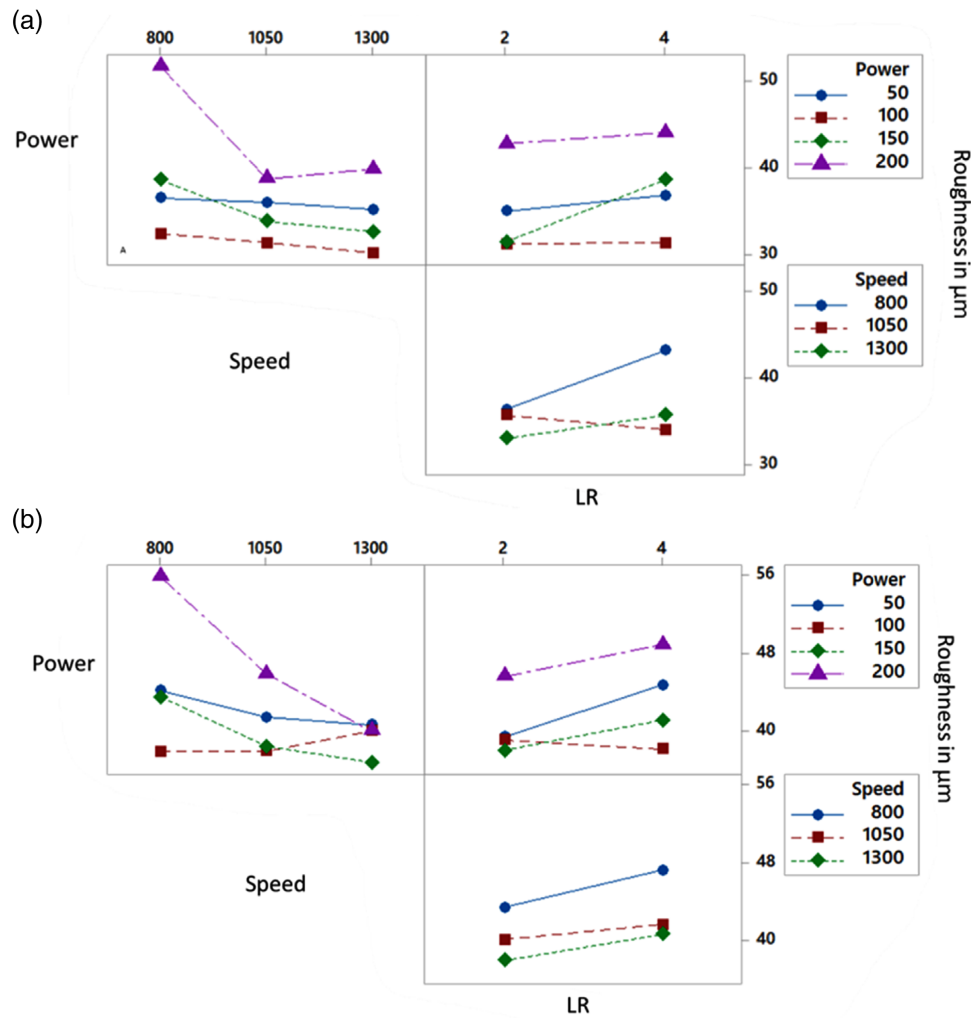


Figure 7. Interaction plot of surface roughness for a) A = 45° and b) B = 40° samples.

roughness of the downskin region varies substantially with build angle, and when printing with varying laser powers and scanning speeds. From the results of the experiments, it is evident that all the samples have a R_a surface roughness greater than 10 μm . This is mainly because of dross formation during the fabrication.

When the linear energy density (LED) is below 0.063 J mm^{-1} , the surface of SLM-fabricated parts is not optimal nor melted completely. This can be seen from the type of defect found on the downskin surface in samples 1–6. The rationale for this is that the melt pool could not completely spread because of the quick solidification time, and the energy was not able to penetrate completely the powder bed causing an escalation in the surface roughness.^[34] When the linear energy density is between 0.063 and 0.154 J mm^{-1} , the SLM process is in the most optimal zone and a minimum in surface roughness was obtained. This is because the laser was capable to melt the powder completely, forming a smooth and continuous track with a sufficient depth of the track which is suitable to form good wettability on the solid substrate. When the energy density is appropriate, the duration of the solidification time is adequate for the molten drop to wet

and spread perfectly with the substrate, while the amount of Marangoni convection is not enough powerful to unsettle the molten pool. There is a decrease in the adherence of the particles and droplets to the deposited track's surface. For the same LED, higher laser power results in a better bonding condition in the neighboring layers, and this results in lower surface roughness. SLM fabrication is in the excessive melting zone when the laser energy density is greater than 0.154 J mm^{-1} . The input energy in this region is very high that significant overmelting takes place, giving rise to defects or powder material loss. Melt tracks become unstable because of stronger metal evaporation and Marangoni convection, resulting in a coarse surface for specimens. These structures lead to an increase in surface roughness.^[1,34] Moreover, it also melts powder whose layer thickness would exceed the designed value for the formation of the downskin surfaces, hereby exceeding the intended (designed) layer.

There is also a considerable relationship between the surface roughness and the scanning speed.^[35] The surface roughness enhances with a higher laser scan speed due to the decrease of the molten layer solidification level. These defects appear in

the molten particle, attached to the powder, and make the solidified form of the laser track. Any instabilities in the melt pool because of the surface tension gradient might affect the inconsistency of the surfaces. Also, in higher printing velocities, this would be harsher and might even result in the formation of droplets and discontinuity (known as balling effect).

The presence of partially melted powders on the downfacing surface cannot be avoided completely. This is caused during the printing process when molten pool or dross met the loose unsupported powder below it. This causes the partial melting of these loose powder particles which leads to attachment or embedment of the loose particles to the downskin surface. This, coupled with dross formation, is the major reason for surface roughness in the downfacing region.

Another observation made is that the 40° samples exhibited a rougher downskin surface than 45° samples. Even though both types of samples are printed on loose powder particles, 40° samples are steeper than 45° samples. As a result, the 45° samples have a smaller overheating zone as some heat could be conducted by the solid bulk of the part. The 40° degree samples dissipate heat less efficiently compared to 45° samples and this is due to the low thermal conductivity of the powder, which creates a bigger melt pool and increases dross.

Surface roughness enhances with an increase in the LR value. This is mainly contributed to heat accumulation near the edges of a layer. When the laser moves to the ending edge of a sample, there is more energy absorbed by the powder due to the insulating powder below it, resulting in a substantial rise in the height of the deposited tracks in this zone. The instability region has a considerable impact on the bonding quality among the neighboring layers, causing evident ripples as well as a rougher surface on the edges.

3.4. Dimensional Accuracy Evaluation

In SLM, heat is dissipated largely by conduction through the solid material; however, downskin surfaces are built on top of powder rather than solid material. Hence, part of the dissipated heat is conducted to the powder bed because of the angle of inclination, producing the adjacent particles to make partial sintering/melting points, and attach to the downskin surface.^[36] This phenomenon is also observed in this study due to the formation of dross and balls on the surface, and it consequently has a significant impact on the sample dimension. As a matter of fact, the formation of these can be attributed to high energy input, which results in the formation of larger melt pools. Consequently, this could cause large dross with less measured roughness, as large melt pools lead to more interconnected melt pools which cannot be detected just by measuring roughness.^[37]

The thickness of the as-built downskin walls is measured at five points along the length of the sample at a 7 mm distance apart and compared with the CAD model (i.e., 10 mm). The difference between the two gives the deviation in a dimension of the built samples. This measurement gives the maximum deviation from the desired geometry due to the undesired attachment of particles. **Figure 8** illustrates the graph of the measured dimension against the energy density corresponding to each sample. The dimensional deviation is calculated as the difference

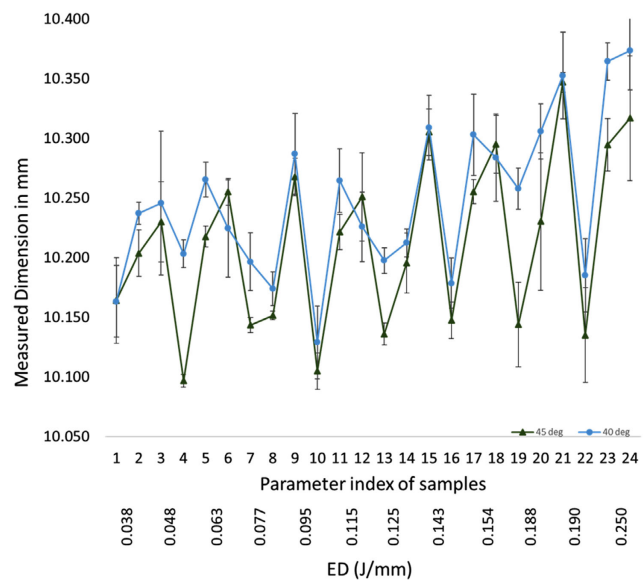


Figure 8. Measured dimension versus linear energy density for samples A (45°) and B (40°).

between the average of measured dimensions and the desired size of the sample (as specified in the CAD file). Although a clear conclusion cannot be made from this graph, samples A and B show a similar trend in the measured dimension, and the deviation is increasing as the energy density is increasing. As visible, there is a periodic increase in deviation for both samples A and B. In particular, for sample A, the deviation increases from samples number 1–3, then drops for 4. Again, this fluctuation repeats from 4 till 6 and drops. So, samples (of A) 1, 4, 7, and so on have the lowest measured dimension, while samples 3, 6, 9, and so on have the highest measured dimension. This trend is also visible in some sets of sample B ({1–3}, {13–15}, {22–24}). This would be because the arrangements of the samples as 1, 4, 7, and so on are positioned at the left end of the build plate, while 3, 6, 9, and so on are placed at the right end of the build plate.

Figure 9a,b shows the graphical plots of interaction between the power, speed, and LR on the deviation of measurement. These are an interaction between power–speed, power–LR, and speed–LR based on deviation values on the right-side Y-axis. As the laser power increases from 50 to 100 W, the deviation decreases and reaches a minimum value. Further increase of the power beyond 100 W increases the dimensional deviation. For a particular power, an increase of LR decreases the deviation. For an LR value of 2, increasing the speed at first decreases the deviation, but causes an increase when increased further. This trend is completely reversed for an LR value of 4.

The result shows that the intermediate power (100 W), intermediate speed (1050 mm s⁻¹), and higher LR (4) are giving the smallest deviation. For roughness, a smaller area of downskin (LR = 2), lower and higher speeds are giving a minimum value, while for dimensional deviation it is exactly the opposite when the area of downskin is large (LR = 4).

An LR value of 4 resulted in a lower dimensional deviation than a value of 2. This is because of the smaller number of pillars formed when using an LR of 4. As it can be seen in Figure 4, an

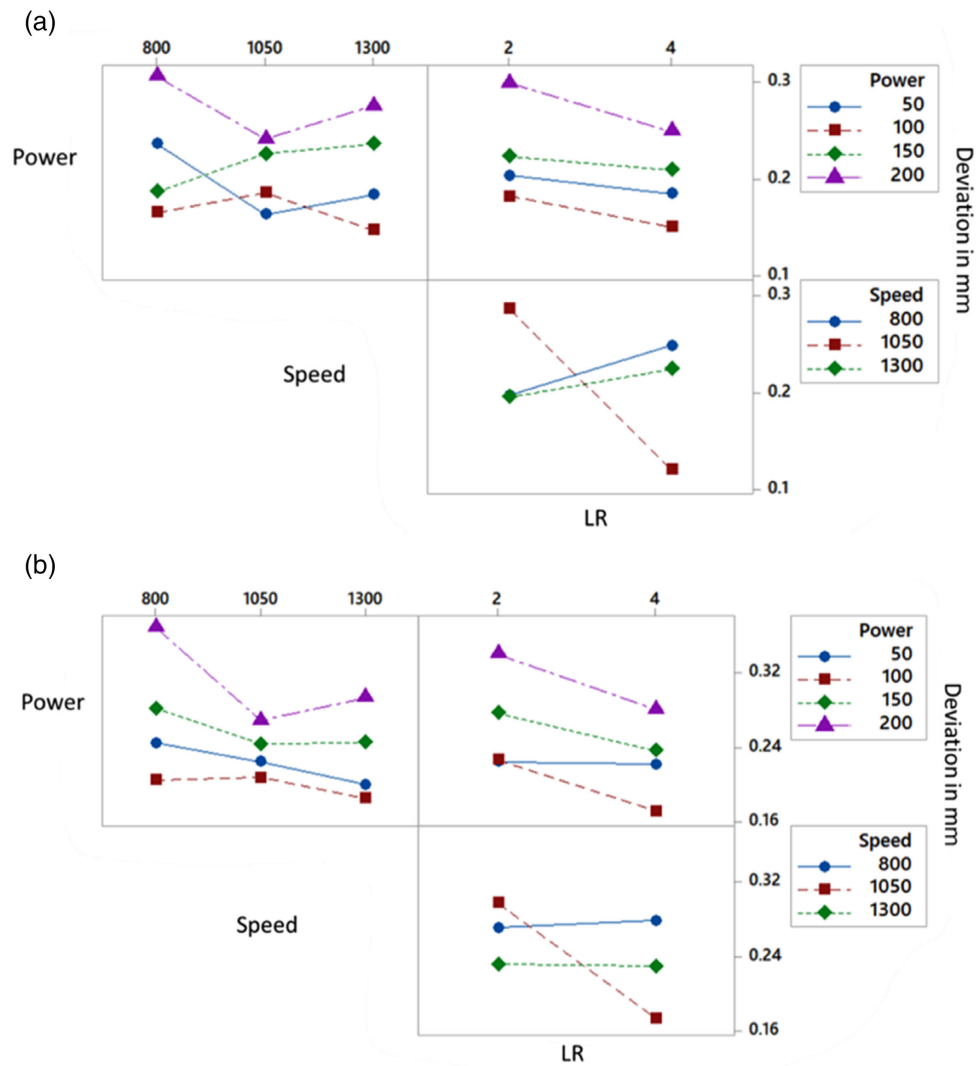


Figure 9. Interaction plot dimensional deviation for a) A = 45° and b) B = 40° samples.

LR value of 4 has more area above the previously formed layer than an LR value of 2. This can help to successfully transfer more heat to previous layers than with a value of 2 and hence reduce the formation of pillars. However, this leads to an increase in the occurrence of other defects like balling as indicated by the surface roughness measurement.

The increased dimension of pillars on the right side of the build plate can also be attributed to the gas flow across the build chamber. The gas flow goes into the build chamber from the right-hand side and exits at the left-hand side. At the right side of the build chamber, the gas flow enters through the porous wall as well as an opening at the bottom of the wall. At the left, the gas leaves the chamber through only an opening at the bottom of the wall. The gas flow speed over the surface of the powder bed is higher on the right side than on the left side. However, in the real case scenario, the validity of this has to be confirmed with further experiments. The change of speed of the gas flow from the inlet to the outlet has to be found out. As the gas flow cools the parts, this difference in speed can cause different cooldown

rates at the left and right sides of the build. The nonuniform cooling rates between the left and right sides of the chamber result in dimensional deviations. The condition of the gas flow—whether it is laminar or turbulent during the printing—is unknown. Possibilities of vortex formation on the right side of the chamber cannot be neglected. Imaging of the inert gas flow inside the commercial SLM machines has not been reported in the literature. The porous wall on the right side of the build chamber can get clogged during the printing due to contaminants inside the chamber. This cannot be detected easily until spatter and dust could be noticed toward the left side of the chamber. Maintaining a uniform gas flow across the build chamber is highly important to obtain accurate builds.

4. Conclusion and Future Works

The research herein involved a study into the effect of process parameters and conditions on the surface roughness and

dimensional accuracy of downfacing surfaces printed by the SLM system. The key takeaway of the research work is as follows: 1) For all samples, the downfacing surface exhibited a rough profile. Laser power, scan speed, and LR are significant factors affecting the roughness. The experimental results show that lower powers, higher scanning speeds, and lower LR values are favorable for lower roughness. 2) Also, the process parameters (i.e., laser power, scanning speed, and LR) have a strong impact on the dimensional deviation of the samples. The results reveal that lower powers, medium speed, and higher LR are found to give the least dimensional deviation. 3) For all samples, the measured thickness is greater than the designed dimension (10 mm). This is due to the attached particles which are melted partially or unmelted. Therefore, finding the optimal printing parameters can minimize the drawbacks of the process. 4) The comparison between the angles of inclination from the build plate shows that surface roughness and deviation increase when the angle decreases from 45° to 40°. 5) An LR value of 2 is found to be more suitable for reducing roughness at the downskin surfaces, while an LR value of 4 gives a lower dimensional deviation.

The limitations of the study are as follows: 1) Challenges in reproducing the results due to variation in the powder quality after each filtering. From the production point of view, it is not feasible to use virgin powder for every print. Repeated use and sieving of the powder can have detrimental effects such as oxide formation, the introduction of contaminants, and a shift in the particle size distribution. It is important to ensure that the spatter and welded particles are efficiently removed. Hence, no two prints can have the same chemical state of powders. 2) The unpredictability of the thermal phenomena inside the build chamber. SLM printing balance between under- and overmelting is easily disrupted by variations in part shape and the number of parts in a single build. Certain build conditions, such as the gas flow distribution, are difficult to keep as a constant and will have an effect when subjected to small changes. 3) Clogging of the porous walls through which gas flow enters the chamber is unpredictable and is not detected until spatter and dust deposition are seen on the left side of the chamber.

The research conducted lays a solid foundation for solving the uncertainties in the downskin region. For future work, the following directions are proposed: 1) An experimental study to measure the gas flow across the inlet and outlet during printing. Gas flow plays a major role in the SLM builds. Therefore, uniform gas flows are expected during the process. Further experiments are required to measure the variation of gas flow and its relation to the measured roughness and dimensional deviations. The effectiveness of spatter removal during the building process needs to be investigated. The relation between locations of the samples on the build plate and interaction with the gas flow is also assumed to be contributing to surface roughness and dimensional deviation. 2) Investigation into the material addition at the tips of samples where the laser is not supposed to reach. There was some material added at the top end tips of some of the samples as shown in Figure 6. This happens in the region where the laser is not supposed to scan. The exact reason is unknown. The author believes that it was due to the defect in the recoater blades. However, further analysis and printing are required to confirm it. The curved region at the end indicates the effect of heat dissipation. Simulation can be used to further investigate it.

3) Numerical representation of the samples. Undulating surfaces were observed on the surface when sandblasting removed the dross, balls, and unmelted particles from the samples in the postprocessing step. A visual inspection could not establish a periodicity. This surface can be investigated further to represent using a Fourier series. Further analysis into the randomness or periodicity can help in predicting the surface anomalies occurring in SLM. 4) Growth rate or pattern of the particles sticking and added to the surface of the downskin as energy density is increased. Pillars attached to the downfacing surface of samples could be observed in Figure 5b. At first glance, the distance between these pillars is random. Further investigations are required to see if there is a relationship between the process parameters and the height of pillars. If a relationship between the growth rate of pillars and process parameters could be achieved, it will help to predict the compensation of dimensional deviations in order to reduce the pillars on the surface.

Conflict of Interest

The authors declare no conflict of interest.

Data Availability Statement

The data that support the findings of this study are available from the corresponding author upon reasonable request.

Keywords

additive manufacturing, Corrax steel, downfacing surfaces, selective laser melting

Received: November 13, 2021

Revised: February 28, 2022

Published online: April 22, 2022

- [1] I. Gibson, D. W. Rosen, B. Stucker, M. Khorasani, D. Rosen, B. Stucker, M. Khorasani, in *Additive Manufacturing Technologies*, Springer Cham, Switzerland, **2021**, 17.
- [2] P. Zarrintaj, H. Vahabi, T. J. Gutiérrez, M. Mehrpouya, M. R. Ganjali, M. R. Saeb, in *Handbook of Polymer Nanocomposites for Industrial Applications*, Elsevier **2021**, pp. 675–685.
- [3] M. Mehrpouya, A. Vosooghnia, A. Dehghanghadikolaei, B. Fotovvati, in *Sustainable Manufacturing*, Elsevier **2021**, pp. 29–59.
- [4] M. Mehrpouya, A. Dehghanghadikolaei, B. Fotovvati, A. Vosooghnia, S. S. Emamian, A. Gisario, *Appl. Sci.* **2019**, 9 3865.
- [5] A. Gisario, M. Kazarian, F. Martina, M. Mehrpouya, *J. Manuf. Syst.* **2019**, 53, 124.
- [6] M. Mehrpouya, A. Gisario, M. Nematollahi, A. Rahimzadeh, K. S. Baghbaderani, M. Elahinia, *Mater. Today Commun.* March, **2021**, 26, 102022.
- [7] U. S. Bertoli, A. J. Wolfer, M. J. Matthews, J.-P. R. Delplanque, J. M. Schoenung, *Mater. Des.* **2017**, 113, 331.
- [8] A. B. Anwar, I. H. Ibrahim, Q.-C. Pham, *Powder Technol.* **2019**, 352, 103.
- [9] B. Vrancken, *Study of Residual Stresses in Selective Laser Melting*, **2016**.
- [10] L. Thijs, B. Vrancken, J. P. Kruth, J. Van Humbeeck, *Advanced Materials, Processes and Applications for Additive Manufacturing*, Vol. 1, **2013**, pp. 21–28.

- [11] K. Mumtaz, N. Hopkinson, *Rapid Prototyping J.* **2009**, *15*, 96.
- [12] Z. Chen, S. Cao, X. Wu, C. H. Davies, in *Additive Manufacturing for the Aerospace Industry*, Elsevier **2019**, pp. 283–299.
- [13] A. Leon, E. Aghion, *Mater. Charact.* **2017**, *131*, 188.
- [14] Z. Chen, X. Wu, D. Tomus, C. H. Davies, *Addit. Manuf.* **2018**, *21*, 91.
- [15] G. Strano, L. Hao, R. M. Everson, K. E. Evans, *J. Mater. Process. Technol.* **2013**, *213* 589.
- [16] J.-P. Kruth, L. Froyen, J. Van Vaerenbergh, P. Mercelis, M. Rombouts, B. Lauwers, *J. Mater. Process. Technol.* **2004**, *149* 616.
- [17] K. Kempen, *Expanding the Materials Palette for Selective Laser Melting of Metals*, PhD thesis, KU Leuven, **2015** https://limo.libis.be/primo-explore/fulldisplay?docid=LIRIAS1673720&context=L&vid=Lirias&search_scope=Lirias&tab=default_tab&fromSitemap=1.
- [18] I. Yadroitsev, I. Shishkovsky, P. Bertrand, I. Smurov, *Appl. Surf. Sci.* **2009**, *255* 5523.
- [19] D. Gu, Y. Shen, *Mater. Des.* **2009**, *30* 2903.
- [20] F. Calignano, *Mater. Des.* **2014**, *64*, 203.
- [21] M. Cloots, L. Zumofen, A. B. Spierings, A. Kirchheim, K. Wegener, *Rapid Prototyping J.* **2017**.
- [22] H. Chen, D. Gu, J. Xiong, M. Xia, *J. Mater. Process. Technol.* **2017**, *250*, 99.
- [23] Y. Lee, W. Zhang, *Addit. Manuf.* **2016**, *12*, 178.
- [24] M. Afrasiabi, C. Lüthi, M. Bambach, K. Wegener, *Appl. Sci.* **2021**, *11* 2962.
- [25] Z. Xiang, L. Wang, C. Yang, M. Yin, G. Yin, *Optik* **2019**, *176*, 68.
- [26] W. Shi, P. Wang, Y. Liu, G. Han, *Metals* **2019**, *9* 385.
- [27] D. Wang, Y. Yang, Z. Yi, X. Su, *Int. J. Adv. Manuf. Technol.* **2013**, *65* 1471.
- [28] C. M. Taylor, I. P. Ilyas, K. W. Dalgarno, J. Gosden, in *International Manufacturing Science and Engineering Conference*, **2007**, 42908, 9.
- [29] R. Mertens, S. Clijsters, K. Kempen, J.-P. Kruth, *J. Manuf. Sci. Eng.* **2014**, *136* <https://doi.org/10.1115/1.4028620>.
- [30] D. Wang, S. Mai, D. Xiao, Y. Yang, *Int. J. Adv. Manuf. Technol.* **2016**, *86* 781.
- [31] Uddeholm, AM Corrax, **2021**, https://www.uddeholm.com/app/uploads/sites/36/2017/08/AM-Corrax-english_1705_e1.pdf (accessed: August 2020).
- [32] F. Petzoldt, H. Pohl, A. Simchi, B. Alcantara, *Met. Powder Rep.* **2006**, *61* 10.
- [33] S. A. Khairallah, A. A. Martin, J. R. Lee, G. Guss, N. P. Calta, J. A. Hammons, M. H. Nielsen, K. Chaput, E. Schwalbach, M. N. Shah, *Science* **2020**, *368* 660.
- [34] T. Yang, T. Liu, W. Liao, E. MacDonald, H. Wei, X. Chen, L. Jiang, *J. Mater. Process. Technol.* **2019**, *266*, 26.
- [35] A. H. Maamoun, Y. F. Xue, M. A. Elbestawi, S. C. Veldhuis, *Materials* **2018**, *11* 2343.
- [36] F. Calignano, *Virtual Phys. Prototyping* **2018**, *13* 97.
- [37] A. Charles, A. Elkaseer, T. Mueller, L. Thijs, V. Hagenmeyer, S. Scholz, *Addit. Manuf.* **2018**, *10* 850.
- [38] H. Vahabi, F. Laoutid, M. Mehrpouya, M. R. Saeb, P. Dubois, *Mater. Sci. Eng. R Rep.* **2021**, *144*, 100604.